HHS Public Access

Author manuscript

Science. Author manuscript; available in PMC 2018 April 27.

Published in final edited form as:

Science. 2017 October 27; 358(6362): 502–505. doi:10.1126/science.aao0350.

Toughening elastomers using mussel-inspired iron-catechol complexes

Emmanouela Filippidi[1,2,*], **Thomas R. Cristiani**[1,3,*], **Claus D. Eisenbach**[1,4], **J. Herbert Waite**[1,5], **Jacob N. Israelachvili**[1,3,6], **B. Kollbe Ahn**[7], and **Megan T. Valentine**[1,2,†]

[1]Materials Research Laboratory, University of California, Santa Barbara, CA 93106, USA

[2]Department of Mechanical Engineering, University of California, Santa Barbara, CA 93106, USA

[3]Materials Department, University of California, Santa Barbara, CA 93106, USA

[4]Institut für Polymerchemie, University of Stuttgart, Germany

[5]Department of Molecular, Cellular and Developmental Biology, University of California, Santa Barbara, CA 93106, USA

[6]Department of Chemical Engineering, University of California, Santa Barbara, CA 93106, USA

[7]Marine Science Institute, University of California, Santa Barbara, CA 93106, USA

Abstract

Materials often exhibit a trade-off between stiffness and extensibility; for example, strengthening elastomers by increasing their cross-link density leads to embrittlement and decreased toughness. Inspired by cuticles of marine mussel byssi, we circumvent this inherent trade-off by incorporating sacrificial, reversible iron-catechol cross-links into a dry, loosely cross-linked epoxy network. The iron-containing network exhibits two to three orders of magnitude increases in stiffness, tensile strength, and tensile toughness compared to its iron-free precursor while gaining recoverable hysteretic energy dissipation and maintaining its original extensibility. Compared to previous realizations of this chemistry in hydrogels, the dry nature of the network enables larger property enhancement owing to the cooperative effects of both the increased cross-link density given by the reversible iron-catecholate complexes and the chain-restricting ionomeric nanodomains that they form.

Despite demands for tough, high-modulus polymer materials, it remains difficult to develop strategies that increase their mechanical strength without sacrificing their maximum elongation and toughness. The traditional approach of incorporating fillers into polymers,

†Corresponding author. valentine@engineering.ucsb.edu.
*These authors contributed equally to this work.

SUPPLEMENTARY MATERIALS
www.sciencemag.org/content/358/6362/502/suppl/DC1
Materials and Methods
Supplementary Text
Figs. S1 to S8
Table S1
References (*27*–*30*)

including nanofillers (1), results in a trade-off between stiffness and extensibility. Recent strategies, such as interpenetrating double and triple networks (2, 3), employ intricate network architectures to efficiently dissipate energy through the mechanically induced rupture of one or more sacrificial networks. Alternatively, energy can be dissipated in single-network architectures by incorporating sliding (4) or sacrificial, reversible cross-links. Examples of the latter include metal coordination (5–7), hydrogen bonding (8), supramolecular systems (9), and ionic or Coulombic interactions (10). Reversible bonding and interpenetrating networks have also been combined, resulting in property enhancements exceeding those of either individual strategy (7, 11). However, to date, these improvements have been limited to soft, low–elastic moduli dry networks ($E < 10$ MPa) (2, 8) or to promising hydrated networks ($E = 35$ MPa) (7).

Our strategy is inspired by the tough polymeric byssal threads used by marine mussels to secure themselves on surfaces to survive the wave-swept intertidal zone. The distal portions of the *Mytilus californianus* and *Mytilus galloprovincialis* mussel threads are composed of cylindrical collagenous cores surrounded by proteinaceous cuticles, which are stiff and extensible, and partially recover after loading (12). The cuticle's chemistry, which contains considerable coordination bonding between the abundant catecholic amino acid 3,4-dihydroxyphenylalanine (Dopa) and iron (III) (13), has inspired numerous efforts (5, 14, 15) that demonstrate enhanced mechanical properties and control of dynamic bonding time scales but have been limited to wet, soft systems such as hydrogels. However, the extended chains of hydrated systems prevent a combination of high stiffness and elongation. Furthermore, water weakens physical interactions that depend on close spatial proximity of interacting groups, such as Coulombic attraction, coordinate bonding, or interchain friction, softening hydrated materials.

In contrast to previous studies, we present a dry polymeric system that uses these sacrificial metal coordination bonds alongside chemical cross-links, resulting in a load-bearing network ($E \approx 184$ MPa) that does not trade off extensibility ($\varepsilon_{max} \approx 150\%$) for stiffness. The iron-catechol coordination bonds provide the additional benefit of being dynamic and spatially reconfigurable with bond strengths comparable to those of covalent bonds (16–18), resulting in a material with both high stiffness and toughness relative to similar networks lacking coordination bonds. The development of a dry polymer that is stiff yet extensible has the potential to substitute for stiff but brittle polymers, especially in impact and torsion-related applications.

To achieve networks of architecture and performance similar to that of the mussel byssal cuticle, a loosely cross-linked amorphous epoxy network with high catechol content (~14 mol % of starting constitutive units) was synthesized and subsequently treated with iron to form dynamic iron-catechol cross-links (Fig. 1 and supplementary materials). The desired network topology was attained by reacting a short-chain bisepoxide [poly(ethylene glycol) diglycidyl ether (PEG-DE)], a monoepoxide carrying a triethylsilyl-protected catechol group (CAT), and a tetrafunctional diamine cross-linker [1,4-diaminobutane (DAB)]. Given the stoichiometry of the starting materials (Fig. 1A and table S1), particularly the ratio of monoepoxide to bisepoxide, a highly branched, slightly cross-linked network is expected (19) (see supplementary materials for details). Networks of similar topology but different

catechol content were obtained by replacing some or all of the CAT monomers by (2,3-epoxypropyl)benzene (BENZ), which is unable to coordinate iron. Curing was performed at a low enough temperature (60°C) to avoid premature deprotection of CAT. High epoxy conversion was confirmed by Fourier-transform infrared spectroscopy (fig. S1), and gelation was confirmed by rheology (fig. S2).

After curing, the protected network was swollen in aqueous solutions, first to deprotect the CAT groups, and second to introduce iron, forming the iron-catechol cross-links (Fig. 1, B to D). To prevent undesirable cross-links due to catechol-catechol oxidative coupling, and thus establish a well-defined network structure, side reactions that deprotected catechols may undergo during iron complexation were avoided by modifying the protocol developed by Fullenkamp *et al.* (20). In our study, deprotection was performed in dilute HCl (pH 2.5) under an argon atmosphere to avoid catechol oxidation. Both Fe^{3+}-mediated catechol oxidation (fig. S3) and Fe^{3+} hydroxide formation were avoided by introducing the swollen deprotected networks to Fe^{3+} in bicine/NaOH-buffered solutions of highly soluble ferric nitrate nonahydrate at pH 7.5. In the Fe^{3+}-catecholate equilibrium, this pH favors the formation of bis-catecholate complexes in particular (fig. S3), as opposed to mono-catecholate complexes (5). Possible counterions to the bis- and tris-catecholate complexes include Na^{+}, excess Fe^{3+}, and charged ammonium groups formed from the diamine cross-linker; any monocomplexes present are likely neutralized with nitrate. Iron coordination also is much faster than catechol oxidation, preventing catechol covalent coupling (20). Furthermore, bicine weakly chelates Fe^{3+}, protecting it from hydroxylation.

The added iron is uniformly distributed [5 to 8 weight %, as measured by inductively coupled plasma–atomic emission spectroscopy and energy-dispersive x-ray spectroscopy (EDX) (Fig. 2B and fig. S4)] and complexed with catechols (confocal resonance Raman spectroscopy, Fig. 2A). In particular, the Raman peak at 512 cm^{-1} has been associated with increased bis- and tris-complexation relative to mono-complexation (5, 13), indicating that many coordinate bonds act as additional cross-linking points. The same cross-linking strategy is used by the mussel (13).

The resulting networks, before and after iron treatment, are amorphous, exhibiting broad glass transitions between −100° and +50°C, as measured by differential scanning calorimetry (DSC) (fig. S5). The amorphous state was further corroborated by the lack of crystalline peaks measured by x-ray diffraction (Fig. 2D), which also rules out the formation of iron oxide precipitates. In the wide-angle scattering regime, where such peaks would be expected, only an amorphous halo resulting from matrix inter-chain scattering is observed (0.42 nm). Iron precipitation was not detected by EDX at the microscale, nor at the nanoscale (down to ~2 nm) probed with scanning transmission electron microscopy (STEM-HAADF–a technique with high atomic number sensitivity) (Fig. 2, B and C). Therefore, any micro- or nanofiller contribution to the mechanical properties of the network is excluded.

However, small-angle x-ray scattering (SAXS, Fig. 2D) shows broad peaks for the deprotected and iron-treated networks. The corresponding distances must be attributed to the correlation distance, r, between electron-rich, catechol-rich hydrogen-bound domains in the deprotected network (r_{depro} = 9.14 ± 0.04 nm) and iron-rich iron-catechol domains in the

iron-treated network ($r_{100\%}$ = 8.57 ± 0.02 nm, Fig. 2E). Similar broad amorphous peaks have been observed in ionomers and attributed to their ionic domains of liquid-like order (21, 22). In these domains, Fe^{3+} complexed with two or three catechols can be induced to exchange ligands by external energy contributions, such as mechanical stress. These domains also restrict network mobility compared to the iron-free networks. Reducing the number density of these domains by halving the catechol content (50% BENZ network), and thus doubling the average chain length between iron-catechol clusters, n, shifts the ionomer peak to a longer average correlation distance ($r_{50\%}$ = 12.2 ± 0.08 nm), as expected from $\langle r^2_{50\%}\rangle = (n_{50\%}/n_{100\%})\langle r^2_{100\%}\rangle$, with $n_{50\%} = 2n_{100\%}$ (see supplementary materials for details).

Uniaxial tensile tests (Fig. 3A, D638 ASTM standard) show the pronounced increase in stiffness and toughness of the iron-treated networks compared with the protected and deprotected networks, without loss of maximum extensibility. Protected samples are perfectly linearly elastic (E_{prot} = 0.240 ± 0.007 MPa). Deprotection causes doubling of the elastic modulus (E_{depro} = 0.45 ± 0.02 MPa) and the emergence of a yield point at strain $\varepsilon \approx 0.2$, both of which may be attributed to catechol-catechol weak reversible hydrogen bonds and preferential segregation of catechols to domains (as supported by SAXS). After yielding, the linear $\sigma(\varepsilon)$ segment has slope S_{depro} = 0.253 ± 0.003 MPa, converging to the stiffness E_{prot}, as both hydrogen bonds and domain structure are disrupted. After iron treatment, the iron-catechol coordination bonds, which have considerably higher dissociation energies than hydrogen bonds, increase the energetic barrier for a chain to detach from a domain. The net effect is an extraordinarily high 770-fold increase in elastic modulus (E_1 = 184 ± 14 MPa); a 58-fold increase in tensile strength, from σ_{prot} = 0.378 ± 0.002 to σ_1 = 21.9 ± 0.8 MPa; and a corresponding 76-fold increase in the yield stress, from 0.084 ± 0.006 to 6.4 ± 0.4 MPa. Accordingly, there is a 92-fold increase in tensile toughness (energy density), from 0.244 ± 0.007 to 22 ± 2 MJ/m^3. As expected for thermoset polymers (23), the yield stress increases with increasing strain rate (Fig. 3B). Exposure to humidity (reversible) or oxidative conditions (irreversible) reduce both the stiffness and extensibility of the network (fig. S8).

Although part of the increase in the iron-treated network's stiffness at room temperature could be attributed to the increase in T_g observed by DSC (fig. S5), dynamic mechanical analysis shows only a small decrease in storage modulus, from $E'_{iron} = 250\ \mathrm{MPa}$ at T = 22°C (N = 1) to $E'_{iron} = 179\ \mathrm{MPa}$ at 28.7°C, where $\Delta T_{iron} = \Delta T_{depro} = T_{room} - T_{g,depro}$ = 36.7°C (fig. S6). Furthermore, increased temperature causes no measurable morphological changes in the static ionomer domains (SAXS, fig. S7), implying no structural rearrangements. Thus, the increase in the breath of the glass transition is perhaps more influential than the value of T_g and reflects an overlap of various relaxation processes due to the emergent dynamic bonds and ionomeric domains.

Upon cyclic loading of iron-treated networks (Fig. 4, A to C), energy dissipation is manifested as prominent hysteresis loops for strains beyond the linear regime. At small applied strains ($\varepsilon_n \leq 30\%$, Fig. 4A) after a loading-unloading cycle, the covalent network and the unbroken coordination bonds preserve shape-memory and entropically drive the network back to the unstretched state. At larger applied strains ($\varepsilon_n \geq 50\%$), residual strain is

observed even after resting intervals of t_{rest} = 90 min. This residual strain originates from the breaking of coordinate bonds during elongation and their reformation at newly accessible sites, resulting in stress-free network chains (illustrated in Fig. 4E). These rearranged random-coil chains, upon release of tension, attempt to hold the network in the deformed shape for entropic reasons and oppose the restoring force of the covalent scaffold's elasticity. Stress relaxation curves (Fig. 4D) corroborate the fast kinetics.

Other stiff, dry systems with reconfigurable architectures, such as self-healing supramolecular polymers where metal ions bridge polymer chains (9), neutralized thermoplastic ionomer resins (24), or thermoplastic polyurethanes (25), rely almost entirely on their respective microstructures. By contrast, the catechol-rich domains in the iron-treated network are not solely responsible for the enhanced mechanical properties. In the deprotected network, despite the presence of catechol-rich domains, the stiffness, strength, and toughness are low. It is the strength of the iron-catechol coordination bonds that amplifies the effect of the nanoscale domains beyond what would be expected (26). The tough mussel byssal cuticle may rely on the cooperation of similar mechanisms.

In this study, we have combined the bioinspired iron-catechol coordination bonds, which are sacrificial and reversible, with the covalent bonds of a cross-linked epoxy network and created a single load-sharing network that is orders of magnitude stiffer, stronger, and tougher than its iron-free precursor. The toughening mechanism is due to the cooperation of dynamic iron-catechol chemistry in a dry environment and the incorporation of ionomeric nanodomains into a cross-linked network for mechanical enhancement.

Supplementary Material

Refer to Web version on PubMed Central for supplementary material.

Acknowledgments

This work was supported by the NSF Materials Research Science and Engineering Centers (MRSEC) DMR-1121053 (E.F., T.R.C., J.H.W., J.N.I., M.T.V.), the Office of Naval Research N000141310867 (B.K.A.), NIH DE-018468 (J.H.W., J.N.I.), and U.S. Department of Energy DE-FG02-87ER-45331 (T.R.C.). Experiments made extensive use of the University of California, Santa Barbara, California NanoSystems Institute–Materials Research Laboratory shared facilities supported by the NSF MRSEC DMR-1121053. We thank Osaka Organic Chemical Industry Ltd. for providing the triethylsilane-protected eugenol epoxide; E. Davidson, C. Monnier, K. O'Hara, and A. Taylor for help with TEM; A. Pallaoro for help with Raman spectroscopy; K. Fields for use of the tensile testing equipment; A. Gallo of Stanford Synchrotron Radiation Lightsource for preliminary data collection and useful discussions regarding the oxidation state of the iron; and T. Mates for help with XPS. Raw data available at https://figshare.com.

REFERENCES AND NOTES

1. Domun N, et al. Nanoscale. 2015; 7:10294–10329. [PubMed: 26006766]
2. Ducrot E, Chen Y, Bulters M, Sijbesma RP, Creton C. Science. 2014; 344:186–189. [PubMed: 24723609]
3. Ducrot E, Creton C. Adv Funct Mater. 2016; 26:2482–2492.
4. Ohmori K, et al. Chem Commun (Camb). 2016; 52:13757–13759. [PubMed: 27797388]
5. Holten-Andersen N, et al. Proc Natl Acad Sci USA. 2011; 108:2651–2655. [PubMed: 21278337]
6. Mozhdehi D, Ayala S, Cromwell OR, Guan Z. J Am Chem Soc. 2014; 136:16128–16131. [PubMed: 25348857]

7. Lane DD, Kaur S, Weerasakare GM, Stewart RJ. Soft Matter. 2015; 11:6981–6990. [PubMed: 26234366]
8. Neal JA, Mozhdehi D, Guan Z. J Am Chem Soc. 2015; 137:4846–4850. [PubMed: 25790015]
9. Burnworth M, et al. Nature. 2011; 472:334–337. [PubMed: 21512571]
10. Sun TL, et al. Nat Mater. 2013; 12:932–937. [PubMed: 23892784]
11. Sun JY, et al. Nature. 2012; 489:133–136. [PubMed: 22955625]
12. Carrington E, Gosline JM. Am Malacol Bull. 2004; 18:135–142.
13. Harrington MJ, Masic A, Holten-Andersen N, Waite JH, Fratzl P. Science. 2010; 328:216–220. [PubMed: 20203014]
14. Barrett DG, et al. Adv Funct Mater. 2013; 23:1111–1119. [PubMed: 23483665]
15. Grindy SC, et al. Nat Mater. 2015; 14:1210–1216. [PubMed: 26322715]
16. Lee H, Scherer NF, Messersmith PB. Proc Natl Acad Sci USA. 2006; 103:12999–13003. [PubMed: 16920796]
17. Xu Z. Sci Rep. 2013; 3:2914. [PubMed: 24107799]
18. Menyo MS, Hawker CJ, Waite JH. Soft Matter. 2013; 9:10314–10323.
19. Cheng KC. J Polym Sci, B, Polym Phys. 1998; 36:2339–2348.
20. Fullenkamp DE, Barrett DG, Miller DR, Kurutz JW, Messersmith PB. RSC Advances. 2014; 4:25127–25134. [PubMed: 25243062]
21. Grady BP. Polym Eng Sci. 2008; 48:1029–1051.
22. Buitrago CF, et al. Macromolecules. 2015; 48:1210–1220.
23. Lesser AJ, Kody RS. J Polym Sci, B, Polym Phys. 1997; 35:1611–1619.
24. Hirasawa E, Yamamoto Y, Tadano K, Yano S. J Appl Polym Sci. 1991; 42:351–362.
25. Qi HJ, Boyce MC. Mech Mater. 2005; 37:817–839.
26. Bellinger MA, Sauer JA, Hara M. Macromolecules. 1994; 27:6147–6155.

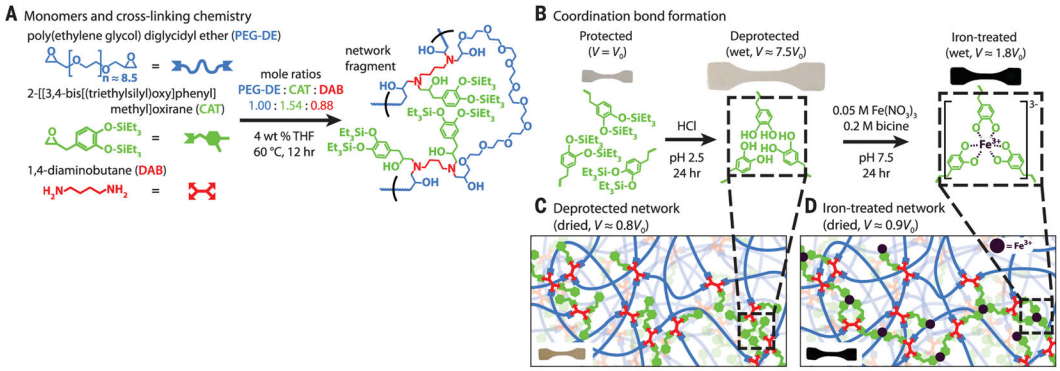

Fig. 1. Monomer and network-formation chemistry

(**A**) The monomers, mole ratios, and curing conditions used in the synthesis of protected catechol-containing networks, and a schematic network fragment showing a CAT cluster. (**B**) A scheme of the cleavage of the silyl protective groups and subsequent iron complex formation, and a depiction of the swelling of a test specimen during the process. (**C** and **D**) Schematics of the network structure before (C) and after (D) iron treatment, illustrating mono-, bis-, and tris-complexation.

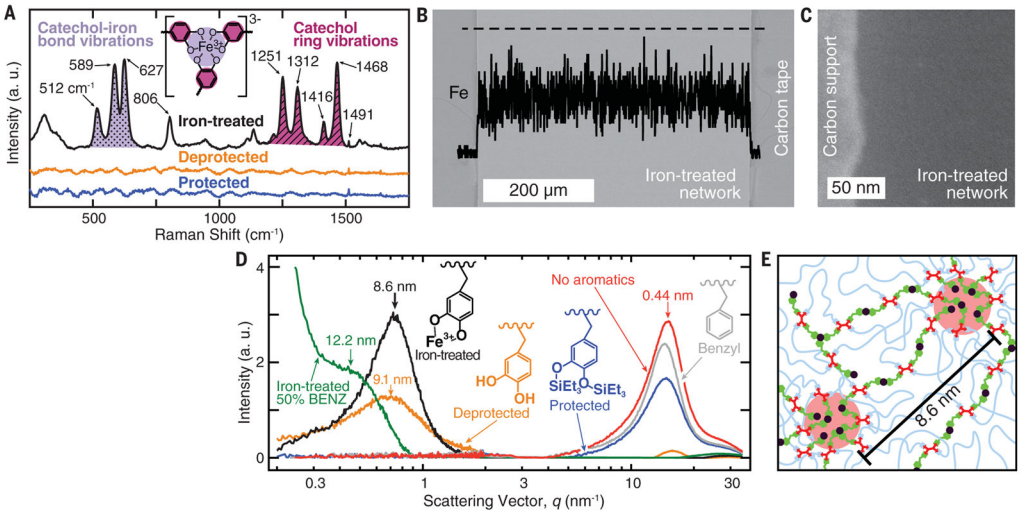

Fig. 2. Characterizing network structure and chemistry in the presence of iron

(**A**) Background-subtracted resonance Raman spectra of protected (blue), deprotected (orange), and iron-treated (black) catechol-containing networks. Both the signal enhancement and characteristic shifts in the shaded regions from 500 to 700 cm^{-1} (purple, dotted) and 1200 to 1500 cm^{-1} (magenta, hashed) confirm iron-catechol coordination. (**B**) Backscattered scanning electron micrograph (background image) and EDX (Fe K) line scan (black curve) along the dashed line of a cross section of a typical sample used for tensile tests. Both show uniform iron diffusion (see also fig. S3). (**C**) High-angle annular dark-field STEM shows no iron aggregates. (**D**) SAXS and wide-angle x-ray scattering (WAXS) of the dry networks. Networks with benzyl (gray), protected catechol (blue), and no aromatic (red) pendant groups show no features in the SAXS regime ($0.1 < q < 2$ nm^{-1}). WAXS peaks (amorphous halo: 0.4197 ± 0.0003 nm) result from interatom matrix scattering. Iron-treated (black) and deprotected (orange) networks have emergent peaks (correlation distances) at 8.57 ± 0.02 and 9.14 ± 0.04 nm corresponding to the development of iron-coordinated and hydrogen-bonded catechol clusters, respectively. (**E**) Schematic of ionomer-like Fe^{3+}-catechol clusters.

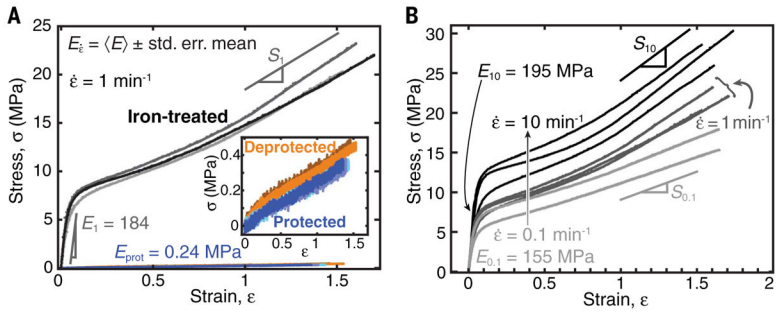

Fig. 3. Uniaxial tensile tests

(**A**) Engineering stress as a function of strain of protected (blue), deprotected (orange), and iron-treated samples (gray); strain rate, $\dot{\varepsilon} = 1\ \text{min}^{-1}$. (**B**) Strain-rate dependence ($\dot{\varepsilon} = 0.1$, 1, and 10 min^{-1}) of iron-treated samples.

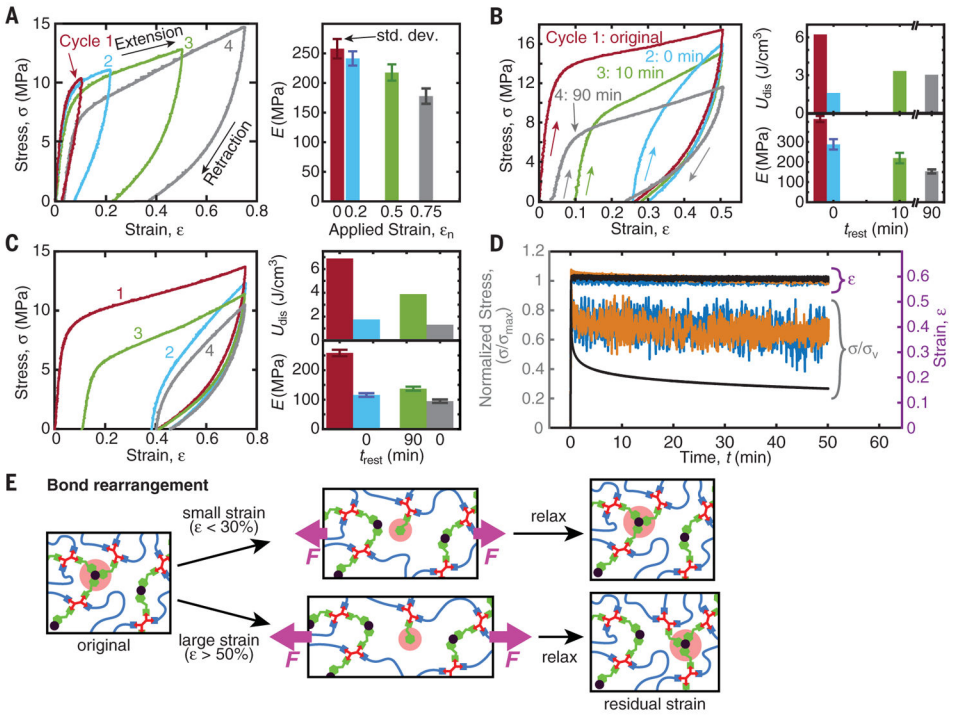

Fig. 4. Cyclic tensile tests and stress relaxation of iron-treated networks show hysteresis and mechanical recovery

(A) Sequential loading-unloading cycles with 30-min rest intervals, t_{rest}, show successful recovery of elastic modulus and no residual strain for $\varepsilon_n < 50\%$. (**B** and **C**) Strain-history dependence with varying rest intervals. Immediate reloading results in reduced toughness (histogram, top) and stiffness (bottom), but a 10-min rest interval results in 90% strain recovery. Longer resting (90 min) does not result in full strain recovery. Softening occurs possibly due to repeated loading or as a result of exposure to low, ambient relative humidity (19 to 20%) (see fig. S8A). Larger applied strain (C) results in reduced strain recovery (72%). (**D**) Stress relaxation for protected (blue), deprotected (orange), and iron-treated (black) specimens indicates the fast elastic and slow viscous responses. σ_{max} = 0.2, 0.3, and 19.3 MPa for protected, deprotected, and iron-treated samples, respectively. (**E**) Proposed mechanism for the strain recovery: At small strains, bonds reform at their original positions; at large strains, bonds migrate further, causing residual strain.